THE JOURNAL OF PHYSICAL CHEMISTRY B

ARTICLE

pubs.acs.org/JPCB

Vibronic Spectra of Perylene Bisimide Oligomers: Effects of Intermolecular Charge-Transfer Excitation and Conformational Flexibility

Fang Gao,[†,§] Yi Zhao,[‡] and WanZhen Liang*[,†]

[†]Hefei National Laboratory for Physical Science at Microscale, and Department of Chemical Physics, University of Science and Technology of China, Hefei 230026, P. R. China

[‡]State Key Laboratory of Physical Chemistry of Solid Surfaces, and Department of Chemistry, Xiamen University, Xiamen, 361005, P. R. China

ABSTRACT: We have recently presented a theoretical study on the temperature-dependent absorption and photoluminescence spectroscopy of rubrene multichromophores by combining the time-dependent long-range-corrected density functional theory with the Frenkel exciton model (Gao; et al. *J. Phys. Chem. A* **2009**, *113*, 12847). The spectra of rubrene multichromophores up to heptamers have been calculated and the effects of exciton−phonon coupling and temperature on the photophysical properties of both H- and J-aggregated oligomers were addressed. However, in that work the contribution of intermolecular charge-transfer excitons (CTEs) to vibronic spectra was not addressed. Here we take into account the effect of CTEs for the absorption and emission spectra of the aggregated perylene bisimide (PBI) oligomers in order to have a quantitative explanation to the experimental absorption and emission spectra of the PBI dyes. The role of intermolecular CTEs is discussed for different intermolecular orientations and distances. The simulations demonstrate that the contribution of CTEs becomes significant when the intermolecular distance is less than 4.5 Å for the $\pi-\pi$ stacked PBI aggregates, and the mixed exciton model is prerequisite to explain the experimentally observed red-shift of the absorption spectra in this case. The large Stokes shift of the emission spectra can be reproduced by our model, and it is induced by the asymmetric nature of the lowest excitonic state of the H-aggregated oligomers. The experimentally observed broad emission bands come from two species with different conformations. As for J-aggregated PBI oligomers, the interactions of FEs induce the red-shift and the increase of the relative intensity of 0−0 peak of the absorption spectra with more aggregated units.

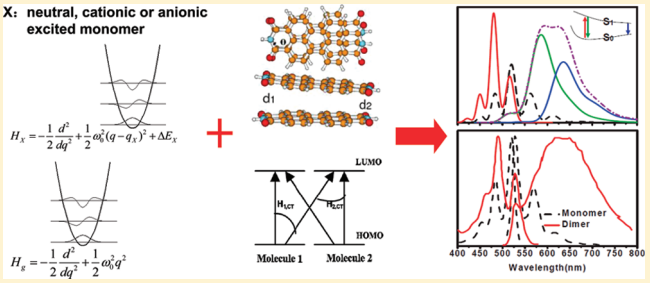

I. INTRODUCTION

Weak, long-range nonbonding intermolecular interactions drive molecules to self-organize, and assemble astonishingly complex, yet functional, biological nanostructures, such as the photosynthetic light-harvesting proteins[1−6] and DNA double-helices.[7−10] Motivated by the functional complexes in nature, a great deal of attention has been devoted to control the self-assembly process of artificial functional dyes in particular with respect to applications in organic electronic or optoelectronic devices. Among functional dyes, PBI dyes have attracted enormous interest due to their favorable properties, such as insolubility and migrational stability, light- and weather-fastness, thermal stability and chemical inertness as well as high tinctorial strength with hues ranging from red to violet, and even black shades.[11] Different types of intermolecular interactions such as hydrogen bonding, $\pi-\pi$ stacking and metal−ligand interactions have been applied to direct the formation of desirable supermolecular structures of PBIs.[12] These noncovalent interactions promote enhanced electronic communication between adjacent chromophores, which mediates electron[13,14] and/or energy transfer.[15−17] The performance of these materials is strongly influenced by intermolecular interactions and the mutual orientation of the single molecules.[18] Detailed knowledge of intermolecular interactions is thus necessary for a rational design of supermolecular functionalities. Insights into these interactions can be gained by studying optical spectra of the aggregates because intermolecular interactions make their imprints on the spectra.

Frenkel exciton (FE) model is a feasible one to predict the spectra of multichromophoes when the chromophores have nonoverlapping charge distributions.[19−24] In such a case, crystal states are constructed from superpositions of neutral Frenkel exciton states. We have recently calculated the spectra of rubrene multichromophores by combining the time-dependent long-range-corrected density functional theory (LRC-DFT) with the Frenkel exciton model,[25] in which the vibronic contribution was taken into account, and found that the spectral behavior of rubrene aggregates is very much dependent on aggregation details. For closely stacking PBI dyes, the noncovalent

Received: August 7, 2010
Revised: December 25, 2010
Published: March 08, 2011

intermolecular interactions may induce the significant overlap between frontier orbitals on adjacent chromophores leading to through-space intercenter full charge delocalization in the stacking direction. The intermolecular charge-transfer excitons (CTEs) may play an important role in the spectra. More complex theoretical models, therefore, are required to account for the delocalized electrons and electron−phonon couplings in the materials. Recently, we have characterized the nature of the low-lying excited states in H-aggregated PBI dyes in terms of LRC-DFT and the mixed intramolecular FE and the intermolecular CTE model.[26] It has been found that the dimer absorption follows closely the spectra of PBI aggregates in solution and strong mixing of FEs and CTEs is demonstrated. However, in that work, the electron−phonon coupling was not taken into account.

In the present work, we extend our previous investigations to incorporate both the vibronic structures and CTEs to have a quantitative explanation of the experimental absorption and emission spectra of the PBIs. We investigate several typical H-aggregated PBI dimers with both vibrationally resolved FE model and mixed FE-CTE model. To reveal the effect of the stacking arrangement on the spectra, we specifically focus on the spectra of the dimers with different mutual orientations, which may tell us how the CTEs influence the spectra by comparing the results from the mixed FE-CTE with those from the pure FE model where the role of CTEs has been fully neglected. In our calculations, all the parameters in the effective model Hamiltonian are gained through ab initio or first-principles calculations.

However, we do note that PBI dye or crystalline PTCDA (3,4,9,10-perylene tetracarboxylic dianhydride) has been theoretically and experimentally studied as one of the most carefully investigated model compounds.[12,23,24,27−43] The experiments have shown that the optical response in the crystalline phase is strongly redshifted, and the photoluminescence line shape is far from a mirror image of the absorption bands, with respect to PTCDA monomers in weakly interacting surroundings like superfluid helium. Parameterized exciton models considering a linear stack of periodically arranged donor and acceptor molecules have been used to explain the experimental spectra. In our work, we consider the finite-size multichromophoric systems, for which the geometrical parameters and the parameters in the effective model Hamiltonian are feasible for a careful ab initio or first-principles treatment. Both the temperature and exciton−phonon coupling effects are included in our model.

The paper is organized as follows: Section II introduces the theoretical models for the spectral calculations. Section III shows DFT calculations of PBI monomer and dimers. Section IV gives out the spectra of PBI oligomers and the concluding remarks are given in Section V.

II. THEORETICAL APPROACHES

A. Effective Hamiltonians. For a multichromophoric system with negligible intermolecular charge overlap, the simplest treatment is to follow Frenkel exciton model

$$\hat{H}^{\mathrm{FE}} = \sum_{ni} \varepsilon_{ni} \hat{B}_{ni}^{\dagger} \hat{B}_{ni} + {\sum_{nimj}}' J_{ni;mj} \hat{B}_{ni}^{\dagger} \hat{B}_{mj} \qquad (1)$$

where $\hat{B}_{ni}^{\dagger}$ now creates a localized Frenkel exciton in level i at molecule n with on-site energy ε_{ni} and $J_{ni;mj}$ denotes the hopping integrals between various localized states. The prime at the summation excludes the terms with $n = m$. Under a first-order approximation in the single excitation theory, the coupling between the two Frenkel excitons on sites n and m is approximated by[44−46]

$$J_{mi,nj} = \langle M_m^* M_n | H | M_m M_n^* \rangle \approx \langle \Psi_m^i \Psi_n^0 | V_{mn} | \Psi_m^0 \Psi_n^j \rangle = \int \mathrm{d}\,\vec{r} \int \mathrm{d}\,\vec{r}\,' \, \rho_m^i(\vec{r}) \frac{1}{|r - r'|} \rho_n^j(\vec{r}\,')$$

Here ρ_m^i and ρ_n^j are the transition densities of the ith excited state of the molecule m and the jth excited state of the molecule n.

One extension of the Frenkel exciton model is to include intermolecular charge-transfer (CT) states. It is well-known that when the molecular orbitals (MOs) of donor and acceptor overlap, the intermolecular CTEs have to be considered. For the sake of simplicity, let us consider a bichromophoric system M_aM_b, two intramolecular localized excitations $|M_a^*M_b\rangle$, $|M_aM_b^*\rangle$, and two charge-localized intermolecular excitations $|M_a^+M_b^-\rangle$, $|M_a^-M_b^+\rangle$ can be formed upon electronic excitation. Two types of electronic configurations mix together to form mixed excitonic states of the bichromophoric system via either purely covalent $\langle M_a^*M_b|H_{\mathrm{DA}}|M_aM_b^*\rangle$, ionic (e.g., $\langle M_a^+M_b^-|H_{\mathrm{DA}}|M_a^-M_b^+\rangle$), or mixed-type (e.g., $\langle M_a^*M_b|H_{\mathrm{DA}}|M_a^+M_b^-\rangle$) interaction.[47,48] The mixed excitonic states possess the natures of both intramolecular and intermolecular excitations.

In a one-dimensional crystal, a localized CT state can be written as

$$|n,f\rangle = C_{n,f}^{\dagger}|0\rangle \qquad (2)$$

meaning that an electron is transferred from molecule n, where it leaves a hole, to molecule $n + f$. If arbitrary electron−hole distances f are allowed, the complete set of the CT basis states $|n,f\rangle$ can describe not only bound CT states but also unbound states corresponding to free charge carriers. If we only consider the CTEs with electron or hole transferred between two nearby sites, the CTE part of the total Hamiltonian can be written as

$$\hat{H}^{\mathrm{CTE}} = {\sum_{nf}}' \varepsilon_f^C \hat{C}_{n,f}^{\dagger} \hat{C}_{n,f} + {\sum_{n,f}}' [M_h(\hat{C}_{n+1,f-1}^{\dagger} \hat{C}_{n,f} + \hat{C}_{n-1,f+1}^{\dagger} \hat{C}_{n,f}) + h.c.] + {\sum_{n,f}}' [M_e(\hat{C}_{n,f+1}^{\dagger} \hat{C}_{n,f} + \hat{C}_{n,f-1}^{\dagger} \hat{C}_{n,f}) + h.c.]$$

The first sum in this notation covers the on-site energies of the CT states, which only depend on the separation f. The second sum includes all nearest-neighbor hops of a hole ("$n \rightarrow n \pm 1$"), and the third term sums the corresponding hops of an electron ("$n + f \rightarrow n + f \pm 1$"). For a linear stack, the FE-CTE mixing part in Merrifield's Hamiltonian[43,49,50]

$$\hat{H} = \hat{H}^{\mathrm{FE}} + \hat{H}^{\mathrm{CTE}} + \hat{H}^{\mathrm{FC}} + \hat{H}^{\mathrm{ph}} + \hat{H}^{\mathrm{ex,phon}} \qquad (3)$$

is expressed as

$$\hat{H}^{\mathrm{FC}} = \sum_n [t_e(\hat{B}_n^{\dagger} \hat{C}_{n,+1} + \hat{B}_n^{\dagger} \hat{C}_{n,-1}) + h.c.] + \sum_n [t_h(\hat{B}_n^{\dagger} \hat{C}_{n+1,-1} + \hat{B}_n^{\dagger} \hat{C}_{n-1,+1}) + h.c.] \qquad (4)$$

Here, the first sum describes the processes in which a nearest

neighbor CT state (separation $f = 1$) is transferred into a Frenkel exciton by a hop of the electron to the position of the hole ("$n \pm 1 \rightarrow^{e} n$"). The reverse transfer of a Frenkel into a CT state is included in the Hermitian conjugated part. The second sum describes the analogous process for the jump of the hole ("$n \pm 1 \rightarrow^{h} n$").

The couplings between FE and CTE, $t_e = \langle M_m^* M_n | H | M_m^+ M_n^- \rangle$ ($t_h = \langle M_m M_n^* | H | M_m^+ M_n^- \rangle$), have to be evaluated, which require to know the wave functions of two localized states (diabatic states). Here we use the approach proposed by Siebbeles[51] and Bredas[52] groups. This method is based on the two-state model, but the electron transitions are only taken place within HOMOs and LUMOs of two isolated neutral monomers. In this one-electron approximation, the electronic coupling is written as

$$t = \frac{h_{12} - \frac{1}{2}(h_{11} + h_{22})S_{12}}{1 - S_{12}^2} \tag{5}$$

Here $h_{ij} = \langle \phi_i | h | \phi_j \rangle$ and $S_{ij} = \langle \phi_i | \phi_j \rangle$, $\phi_{1(2)}$ denotes the LUMOs or HOMOs of two monomers, and h denotes the one-electron effective Hamiltonian. The approach is thus reasonable for the LUMO(HOMO) being well separated from LUMO+1-(HOMO−1) of a monomer. This condition is satisfied in our system. Otherwise, it may be extended to include two or more orbitals.[53] In the above description, the Hamiltonian is only considered for an isolated dimer. In the organic thin films and crystals, however, the dimer is surrounded by other molecules. This environment effect on the electronic coupling can be taken into account by choosing a larger system incorporating both the dimer and the surrounding molecules.[52]

The last two parts of total Hamiltonian of eq 3 are related with phonon and the exciton−phonon couplings

$$\hat{H}^{\mathrm{ph}} = \sum_n \hbar\omega_0 \hat{a}_n^\dagger \hat{a}_n \tag{6}$$

$$\hat{H}^{\mathrm{ex,phon}} = \sum_n \hat{B}_n^\dagger \hat{B}_n \hbar\omega_0 \xi_F (\hat{a}_n^\dagger + \hat{a}_n) + \sum_{n,f} \hat{C}_{n,f}^\dagger \hat{C}_{n,f} \hbar\omega_0 [\xi_h (\hat{a}_n^\dagger + \hat{a}_n) + \xi_e (\hat{a}_{n+f}^\dagger + \hat{a}_{n+f})] \tag{7}$$

Here, we only consider a single phonon mode on each molecular site. $a_n(a_n^\dagger)$ is the annihilation (creation) operator of the phonon on the molecular site n. ω_0 is the frequency of the phonon mode and $\xi_{F(h,e)}$ represents the exciton−phonon coupling strength. In the calculation of the exciton−phonon coupling, one usually starts from normal mode coordinates. Considering an aggregate consisting of p monomers, the total excitonic state Hamiltonian can be written as

$$H_e = \begin{pmatrix} \mathrm{FEs} & \mathrm{CTE-FE} \\ \mathrm{FE-CTE} & \mathrm{CTEs} \end{pmatrix} \tag{8}$$

One can alternatively write the diagonal parts of the Hamiltonian (FEs and CTEs) in the configuration space as

$$H_n^{\mathrm{FE}}(q_1,\ldots,q_p) = -\frac{1}{2}\frac{\partial^2}{\partial q_n^2} + \frac{1}{2}\omega_0^2 (q_n - q_n^{\mathrm{F}})^2 + \varepsilon_n + \sum_{l\neq n}^{p} \left(-\frac{1}{2}\frac{\partial^2}{\partial q_l^2} + \frac{1}{2}\omega_0{}^2 q_l{}^2 \right) \tag{9}$$

$$H_{n^+m^-}^{\mathrm{FE}}(q_1,\ldots,q_p) = -\frac{1}{2}\frac{\partial^2}{\partial q_{n^+}^2} + \frac{1}{2}\omega_0{}^2 (q_{n^+} - q_{n^+}^h)^2 - \frac{1}{2}\frac{\partial^2}{\partial q_{m^-}^2} + \frac{1}{2}\omega_0{}^2 (q_{m^-} - q_{m^-}^e)^2 + \varepsilon^{\mathrm{CT}}(n^+m^-) + \sum_{l\neq n,m}^{p} \left(-\frac{1}{2}\frac{\partial^2}{\partial q_l{}^2} + \frac{1}{2}\omega_0{}^2 q_l{}^2 \right) \tag{10}$$

where subscript "$n^{+(-)}$ denotes the ionized states of molecule n, $q_{n(+,-)}$ represents the mode coordinate on the molecule n, $q_{n(+,-)}^{F(h,e)}$ is the corresponding equilibrium geometry of the neutral excited (ground ionic) state, ε_n is the 0−0 transition energy and $\varepsilon_{n+m-}^{\mathrm{CT}}$ is the energy of the corresponding charge-transfer state formed by a hop of the electron from molecule n to molecule m. The exciton−phonon coupling $\xi_{F(h,e)}$ is related to $q^{F(h,e)}$ by

$$\xi_{F(h,e)} = \sqrt{\frac{\omega_0}{2}} q^{F(h,e)} \tag{11}$$

B. Formula for the Vibronic Spectra. The ground state Hamiltonian of the complex consisting of p monomers is assumed as

$$H_g(q_1,\ldots,q_p) = \sum_{l=1}^{p} \left(-\frac{1}{2}\frac{\partial^2}{\partial q_l{}^2} + \frac{1}{2}\omega_0{}^2 q_l{}^2 \right) \tag{12}$$

Combined with the excitonic state Hamiltonian H_e, two correlation functions for linear response spectroscopy, $C_a(t)$ and $C_e(t)$ can be gained

$$C_a(t) = \frac{Tr[e^{-\beta H_g} e^{iH_g t/\hbar} \mu e^{-iH_e t/\hbar} \mu]}{Tr[e^{-\beta H_g}]} \tag{13}$$

and

$$C_e(t) = \frac{Tr[e^{-\beta H_e} e^{iH_e t/\hbar} \mu e^{-iH_g t/\hbar} \mu]}{Tr[e^{-\beta H_e}]} \tag{14}$$

Here $\beta = 1/k_b T$, and subscripts "a" and "e" correspond to absorption and emission, respectively. $\mathrm{Tr}(\cdots)$ in $C_a(t)$ and $C_e(t)$ is taken with respect to $|g\rangle$ and $|e\rangle$, respectively, and μ is transition-dipole operator

$$\mu = |g\rangle \mu_{ge} \langle e| + |e\rangle \mu_{eg} \langle g| \tag{15}$$

where $|g\rangle$ denotes the eigenstate of the ground state Hamiltonian $H_g(q_1,\cdots,q_p)$ and $|e\rangle$ is the coupled excitonic state gained by diagonalizing the excitonic state Hamiltonian

$$H_e = \begin{pmatrix} \mathrm{FEs} & \mathrm{CTE-FE} \\ \mathrm{FE-CTE} & \mathrm{CTEs} \end{pmatrix}$$

$|e\rangle$ is finally expressed as a linear combination of FEs and CTEs, and the transition dipole moments between $|g\rangle$ and CTEs are zero while those between $|g\rangle$ and FEs are not zero. For example, the transition dipole moment between $|g\rangle$ and the Frenkel exciton on site n, which is the eigenstate of the Hamiltonian $H_n^{\mathrm{FE}}(q_1, \ldots, q_p)$, is just that between the ground state and excited state of monomer n. So the relative orientations of the monomers will lead to geometry factors through transition-dipole operator.

The optical absorption cross section $\alpha(\omega)$ and emission cross section $\beta(\omega)$ are separately obtained from

$$\alpha(\omega) \propto \omega \int_{-\infty}^{\infty} dt \exp(i\omega t - \gamma|t|) C_a(t) \quad (16)$$

and

$$\beta(\omega) \propto \omega^3 \int_{-\infty}^{\infty} dt \exp(-i\omega t - \gamma|t|) C_e(t) \quad (17)$$

III. PROPERTIES OF MONOMERS AND DIMERS

A. Displacement Parameters and Huang−Rhys Factors for Internal Vibrations. The equilibrium geometries of ground states of PBI monomer and its ionized counterparts are calculated at the B3LYP/SVP theoretical level while that of the excited state of the monomer is calculated at the TD-B3LYP/SVP theoretical level within the TURBOMOLE software package.[54] And the normal coordinates and vibrational frequencies of the ground states of the ionized monomers and the excited state of the monomer are all assumed to be the same as those of the ground state of the monomer which are calculated at the B3LYP/SVP theoretical level. The SVP basis set is comparable to 6-31G(d).

The deformation patterns for ionized and excited molecules are projected onto the complete set of vibrational eigenvectors giving in each case the vibronic coupling constants. The reorganization energy λ_k of each mode ω_k is related to its Huang−Rhys factor S_k by

$$\lambda_k = S_k \omega_k \quad (18)$$

where the latter is sometimes expressed in terms of the displacement parameter $q_{e(k)}$ as $S_k = {}^1/_2 \omega_k q_{e(k)}{}^2$. For the mode frequencies, we apply a scaling factor of 0.973 adequate for the B3LYP functional. While in the observed spectra of dissolved chromophores, the various internal vibrations are not resolved, but due to the large Gaussian broadening arising from a fluctuating shell of surrounding solvent molecules, they merge into a single vibronic progression. Therefore, we compress the detailed information obtained from the projection of the deformation patterns onto the vibrational eigenvectors into an effective mode with an effective Huang−Rhys factor[55]

$$S = \frac{\lambda}{\omega_0} = \frac{\sum_k \lambda_k}{\omega_0} \quad (19)$$

$$\omega_0 = \sqrt{\frac{\sum_k \omega_k{}^4 q_{e(k)}{}^2}{\sum_k \omega_k{}^2 q_{e(k)}{}^2}} \quad (20)$$

where the sums are calculated over the range 900−1800 cm^{-1} centering around C−C stretching mode.

The calculated Huang−Rhys factors in the different charge states and in the relaxed excited geometry are summarized in Table 1. As we can see, the energies of the effective modes deduced from the different deformation patterns of ionized and excited states deviate only by a few percent. Therefore the parameters: $\hbar\omega_0$ = 0.180 eV, q^h = 9.1598/(hartree)$^{1/2}$, q^e = 12.7682/(hartree)$^{1/2}$, and q^F = 12.3113/(hartree)$^{1/2}$ are used in the following calculations.

Table 1. Effective Internal Vibration for PBI, with Huang−Rhys Factors S^- and S^+ of the Ionized States Obtained with DFT, and the Huang−Rhys Factor in the Relaxed Excited Geometry with TD-DFT, All at the B3LYP/SVP Level[a]

mode	cation	anion	excited
$\hbar\omega_k$ (cm^{-1})	S_k^+	S_k^-	S_k
211.9	0.001	0.000	0.001
225.3	0.152	0.034	0.281
395.4	0.126	0.205	0.013
468.9	0.015	0.000	0.009
537.3	0.001	0.111	0.082
639.4	0.075	0.006	0.022
722.6	0.001	0.000	0.000
727.2	0.028	0.005	0.011
817.4	0.016	0.006	0.000
1055.7	0.000	0.029	0.006
1173.0	0.003	0.000	0.003
1272.9	0.000	0.024	0.004
1274.9	0.000	0.002	0.000
1297.5	0.003	0.001	0.004
1298.7	0.110	0.040	0.140
1372.9	0.001	0.154	0.065
1395.1	0.001	0.000	0.001
1400.2	0.054	0.044	0.078
1448.8	0.028	0.004	0.020
1582.9	0.044	0.051	0.101
1604.7	0.004	0.143	0.082
1761.8	0.001	0.001	0.000
1766.4	0.031	0.056	0.001
S	0.2775	0.5392	0.5013
$\hbar\omega_0$ (eV)	0.1812	0.1860	0.1800

[a] Only the modes with $S > 0.001$ are shown for clarity.

B. Couplings among the Excitons of Parallel H-Aggregated Dimers. Table 2 lists the parameters in the exciton model for parallel H-aggregated dimers with different intermolecular distances, which come from TD-ωB97X-D[56] (μ=0.20 a_0^{-1}, C_{HF} = 0.22) (the LRC hybrid functional with damped dispersion correction) calculations. These parameters will be used in the following to calculate the vibronic spectra. And the cases for other types of oligomers will be mentioned separately in this paper. The site energy of localized intramolecular exciton is set to be 2.7539 eV.

IV. SPECTRA OF OLIGOMERS

In this section, the spectra of H-aggregated and J-aggregated oligomers shown in Figures 1 and 5 are calculated.

A. Parallel H-Aggregated Dimers. The calculated absorption spectra of the H-aggregated dimers with different intermolecular distances are shown in Figure 2, and the emission spectra at the temperature T = 0 and 300 K are shown in Figures 3 and 4, respectively. The parameters of FE model are the same as those of the mixed FE-CTE model except that the electron and hole transfer integrals are both set to zero, and the spectra resulted from the two models are put together for comparison.

As we can see from Figure 2, when the intermolecular distance is larger than 4.5 Å, the spectra produced by the mixed FE-CTE

Table 2. Vertical Excitation Energies of Dimer with Different Intermolecular Distances at TD-ωB97X-D/6-311G* Theoretical Level[a]

d (Å)	S_1	S_2	S_3	S_4	ε^{CT}	$\lvert t_h \rvert$	$\lvert t_e \rvert$	J
3.5	2.0289 (0.0)	2.8609 (1.087)	2.9557 (0.084)	3.4739 (0.0)	2.9058	0.336	0.350	0.135
4.0	2.4492 (0.0)	2.8512 (1.195)	3.1248 (0.006)	3.2750 (0.0)	3.0962	0.149	0.161	0.120
4.5	2.6033 (0.0)	2.8410 (1.232)	3.2894 (0.001)	3.3189 (0.0)	3.2723	0.065	0.073	0.103
5.0	2.6527 (0.0)	2.8315 (1.251)	3.4376 (0.0)	3.4421 (0.0)	3.4281	0.028	0.033	0.090
6.0	2.6797 (0.0)	2.8153 (1.314)	3.6904 (0.0)	3.6905 (0.0)	3.6841	0.001	0.013	0.063
7.0	2.6988 (0.0)	2.8022 (1.352)	3.7980 (0.0)	3.8028 (0.0)	3.7970	0.001	0.003	0.053

[a] The four states shown in this table just come from the electronic transitions from HOMO−1 (HOMO) to LUMO (LUMO+1) of the dimers. The first and second singlet excitation energies of monomer are 2.7539(0.754) and 3.7958(0.0) eV, respectively. The values in parentheses are the oscillator strengths of the corresponding excited states.

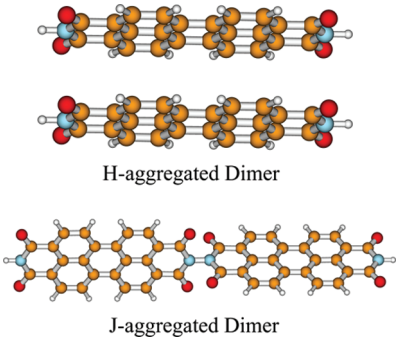

Figure 1. H-aggregated and J-aggregated dimers.

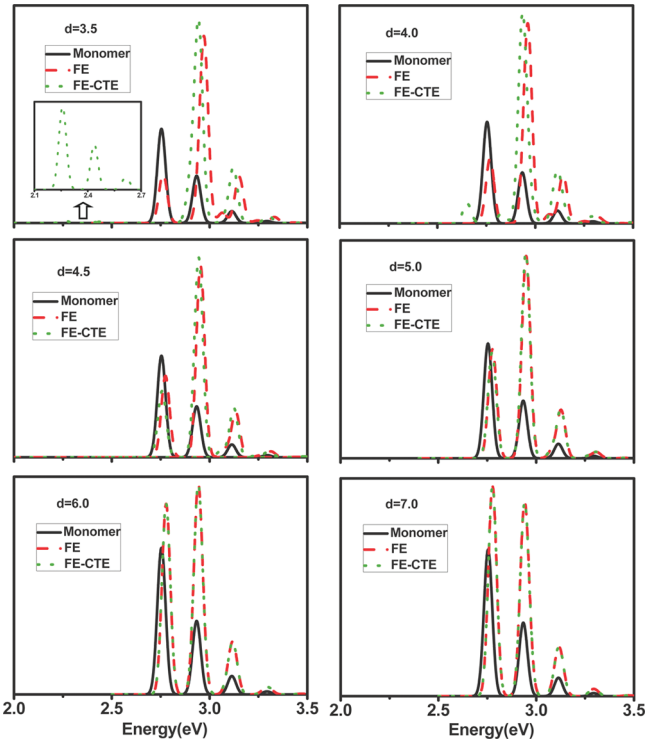

Figure 2. Calculated absorption spectra of PBI dimer at different intermolecular distances with the FE model and the mixed FE-CTE model. The data in the insert figure is magnified by about 35 times.

model are the same as those produced by the FE model. This is easy to understand since in this case the intermolecular CTE states lie much highly above the intramolecular localized excited states, the coupling between FEs and CTEs is weak, and thus the role of CTEs on the spectra can be ignored. However, when the intermolecular distance is less than 4.5 Å, the role of CTEs on the spectra is significant.[26] One can observe obvious spectral differences in this case: the absorption bands produced by the mixed FE-CTE model are broader than those produced by the FE model. Compared with the absorption spectra of monomer, the dimer absorption bands by the mixed FE-CTE model spread to the low energy side while those by the FE model are confined to the high energy region.

From the calculated vertical excitation energies shown in Table 2, we observe that the optically allowed absorption band of H-dimer should always show blue-shift comparing with the monomer's absorption. However, when the vibronic contribution is taken into account as in our model, each electronic excited state will spread to one phonon band, and there are several excitonic states in each phonon band. These excitonic states have different symmetry, leading to the transition from the ground state to these excitonic states either optically allowed or optically forbidden. The first optically allowed excitonic state will become lower than the first electronic excited state of the monomer when the intermolecular distance is small. Therefore the lowest absorption band center at the lower energy's position than that of the monomer in this case. Some description about the non-Condon behavior has been given in our previous paper.[25]

Comparing Figures 3 and 4, we can see that the transition near 0−0 band is absent in the emission spectra at 0 K and appears at 300 K, which can be explained by the energy-level intervals and the temperature-induced alternations of populations of the vibrational states.[25] The rising temperature makes the higher-lying vibronic states populated. These higher-lying vibronic excitonic states may have symmetry different from the lowest excitonic state, which make the transitions near 0−0 band become optically allowed. This behavior (the intensity of transitions near 0−0 band increases with temperature) is in agreement with the experimentally observed temperature-dependent PL behavior of H-aggregated oligomer 2b in ref 38. The same phenomena as in Figure 2 can be observed in both Figure 3 and Figure 4: When the intermolecular distance is beyond 4.5 Å, the two models produce almost the same spectra; However, when the intermolecular distance is less than 4.5 Å, there are differences: the emission spectra gained by FE model show a blue-shift compared with those by mixed FE-CTE model. In the case that the CTEs play important role in the dimer, the emission produced by the mixed FE-CTE model is obviously weaker than that by the FE model, which is due to the nonemissive nature of the CTEs.

In both the absorption and emission spectra of parallel H-dimers, the lowest absorption/emission band centeres at the

dx.doi.org/10.1021/jp107449v |J. Phys. Chem. B 2011, 115, 2699–2708

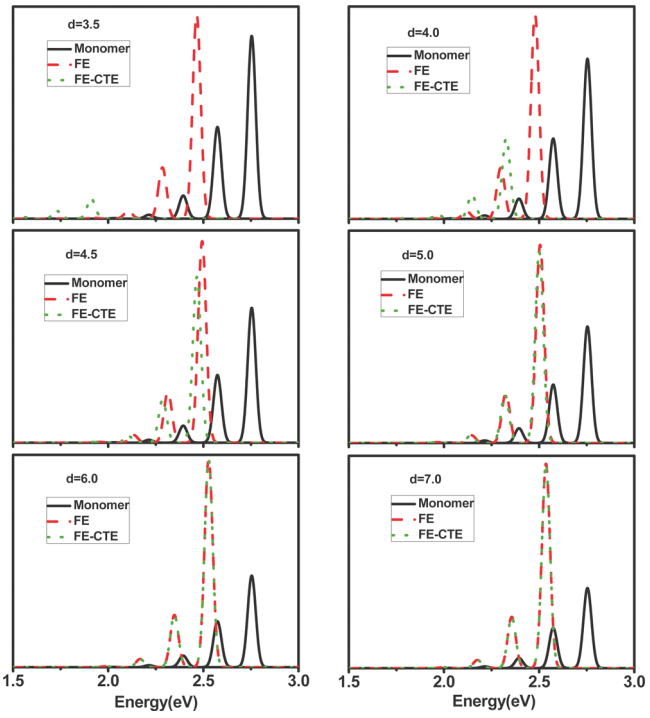

Figure 3. Calculated emission spectra of PBI dimer at different intermolecular distances with FE model and the mixed FE-CTE model at T = 0 K. The intensity of the dimer emission spectra has been magnified by 10 times for comparison.

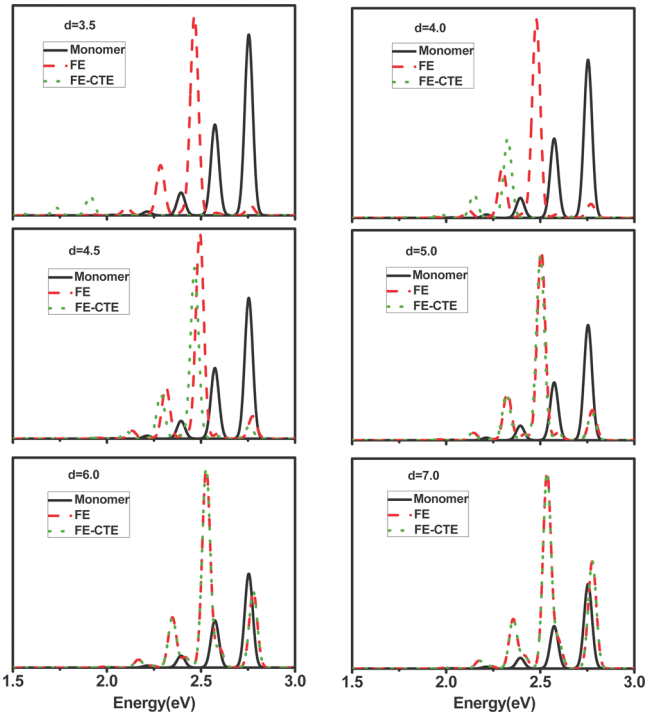

Figure 4. Calculated emission spectra PBI dimer at different intermolecular distances with FE model and mixed FE-CTE model at T = 300 K. The intensity of the dimer emission spectra has been magnified by 10 times for comparison.

lower energy's position than that of the monomer when the intermolecular distance is less than 4.5 Å. This behavior has been attributed to the contribution of CTEs in our model. FEs and CTEs coupled to produce the mixed states with definite symmetry, which will induce some interesting phenomena. The emission intensity of the monomer is about ten times larger than that of this H-aggregated dimer while the emission intensity of the J-aggregated dimer is comparable to that of the monomer which will be shown in Figure 7 in subsection IVC. This difference is just induced by the different symmetry of the dimer's excitonic states. As the emission from the lowest excitonic state dominates in the spectra, the transition from the first dimer excitonic state to the ground state will be taken as an example in the following to demonstrate the difference of the emission intensities. The first excitonic state can be expressed as a linear combination of Frenkel excitons and charge-transfer excitons. As the transition from CTEs to the ground state carries zero oscillator strength, here only the FE components are written out

$$|e\rangle = \sum_{n_3,n_4} (C_{1,n_3,n_4}|1,n_3,n_4\rangle + fC_{1,n_3,n_4}|2,n_3,n_4\rangle)$$

The first excitonic state of H-aggregated dimer is symmetric while that of J-aggregated dimer is antisymmetric, which is shown in ref 25. So here $f = -1$ just holds for H-aggregated dimer while $f = 1$ holds for J-aggregated dimer. $|1,n_3,n_4\rangle$ means the Frenkel exciton located at monomer 1, and n_3 and n_4 are the vibrational quanta of monomer 1 and monomer 2, respectively. The intensity of the transition from $|e\rangle$ to $|g\rangle = |0,n_3,n_4\rangle$ is proportional to the following integral:

$$\langle g|\mu|e\rangle = \langle 0,n_1,n_2|\mu|\sum_{n_3,n_4}(C_{1,n_3,n_4}|1,n_3,n_4\rangle + fC_{1,n_3,n_4}|2,n_3,n_4\rangle)\rangle$$

$$= \mu\sum_{n_3}(C_{1,n_3,n_2}\langle n_1|n_3\rangle_{ge} + fC_{1,n_3,n_1}\langle n_2|n_3\rangle_{ge})$$

here the subscript "ge" means the Franck−Condon integral of the monomer. When the ground state $|0,n_3,n_4\rangle$ is symmetric (when $n_1 = n_2$), $\langle g|\mu|e\rangle = \Sigma_{n_3}\mu(1 + f)C_{1,n_3,n_1}\langle n_1|n_3\rangle_{ge}$, so the transition from the first excitonic state to the symmetric ground state is forbidden for H-aggregated dimer. For the asymmetric ground state $|0,n_1,n_2\rangle$ (when $n_1 \neq n_2$), the transition will be observed, but the transition intensities differ due to the different values of f for H- and J-aggregated dimers.

From both the absorption and emission spectra, we can see that the relative intensity of 0−0 transition increases with the intermolecular distance. When the intermolecular distance approaches infinity, the relative intensity of 0−0 transition will be the same as that of monomer.

B. Nonparallel H-Aggregated Dimer. Many H-aggregated PBI oligomers have been synthesized.[38,40−42] In order to get a clear understanding toward the photophysical properties of these oligomers, we optimize the geometries of ground state and the first excited singlet state of the rigidly linked PBI dimer as shown in the top panel of Figure 5 at HF/3-21G and CIS/3-21G theoretical levels within GAUSSIAN 03 program package,[57] respectively. Then the corresponding geometries of the simplified dimer are extracted. Comparing the optimal structure of S_1 state with that of ground state, we find that the two molecular planes are not parallel to each other for both states, and the relative intermolecular rotational angle becomes smaller, and the interplanar distance decreases at S_1 state. We then perform calculations at ωB97X-D($\omega = 0.20a_0^{-1}$)/6-31G(d) level for these two simplified dimers within the quantum chemistry package Qchem.[58] The following parameters are obtained: (a) for S_0 optimal geometry, J = 103.58 meV, ε^{CT} = 3.35 eV, t_e = 43.5 meV,

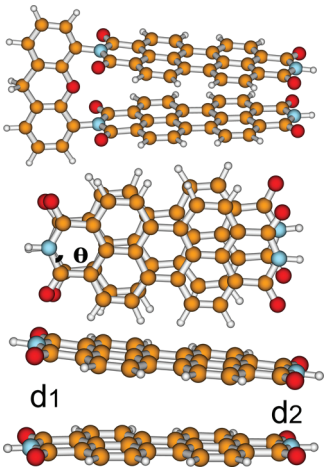

Figure 5. Top panel: the geometry to be optimized. Middle and bottom panel: the simplified dimer geometry from the top view and the side view. The structural parameters of the optimized ground-state geometry at HF/3-21G level: $\theta = 12.90°$, $d_1 = 4.57$ Å, $d_2 = 3.32$ Å. The structural parameters of the optimized S_1 state geometry at CIS/3-21G level: $\theta = 7.16°$, $d_1 = 4.47$ Å, $d_2 = 3.52$ Å.

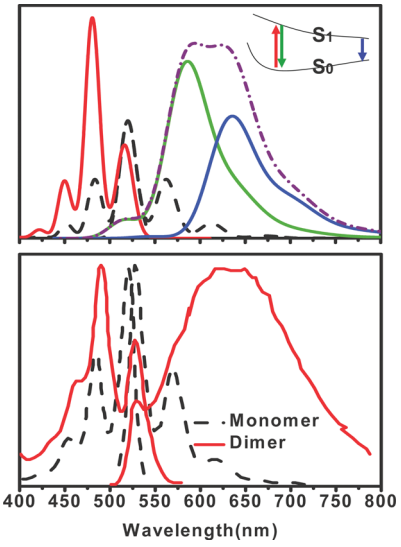

Figure 6. Simulated (the top panel) and experimental[40] (the bottom panel) spectra in 2-Me-THF of PBI monomer and its H-aggregated dimer at room temperature. In order to compare with the experiment, the simulated spectra are shifted down about 0.3708 eV. The intensity of the simulated dimer emission spectra is multiplied by 10 for comparison. In the top panel, the dimer absorption spectra are calculated at the S_0 optimal geometry, and the dimer emission spectra are calculated at the S_0 and S_1 optimal geometries as they both contribute to the total emission spectra.

$t_h = -2.3$ meV; (b) for S_1 optimal geometry, $J = 127.67$ meV, $\varepsilon^{CT} = 3.10$ eV, $t_e = 147.1$ meV, $t_h = -159.1$ meV. The energies of CTEs (ε^{CT}) are gained with the constrained DFT (CDFT) approach[59] at B3LYP/6-31G(d) level. In the simulation of the absorption spectra, the optimal S_0 geometry is adopted. In agreement with the experiment, the intensity of 0−0 peak in the absorption spectra decreases upon aggregation.

The emission spectra for the two dimers are also shown in Figure 6. In the experiment, the dimer has a very broad emission band in low energy region which indicates a large Stokes shift,

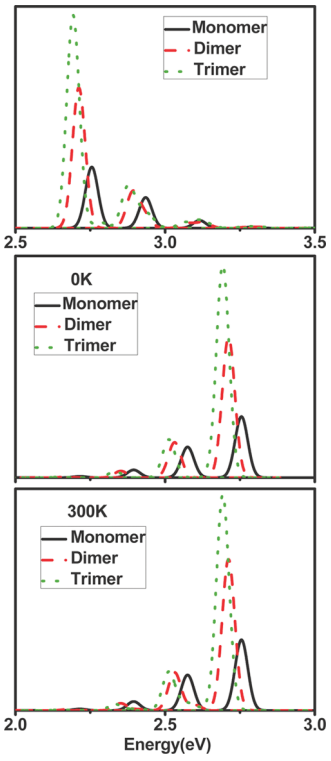

Figure 7. Calculated spectra of J-aggregated oligomers shown in Figure 1 and the oligomers contain two or three PBI units. The emission spectra are at $T = 0$ and 300 K.

and there is a weak peak in the high energy region and the total photoluminescence line shape is far from a mirror image of the absorption bands. And these features can all be well reproduced by just adding the emission spectra produced from S_0 and S_1 optimal geometries. The CTEs of S_1 optimal geometry are below those of S_0 optimal geometry leading to relatively stronger FE-CTE mixing, and thus leads to lower-energy emission. The dimer will slow relax to S_1 optimal geometry after photoexcitation via intermolecular motion. The experiments found two quite different emission lifetimes:[38,40] the shorter one is tens of picoseconds and the longer one is tens of nanoseconds. This indicates a slow excited-state geometrical relaxation with large change of intermolecular relative orientation, which may finally produces the large stokes shift and the broad emission band. Therefore we come to a conclusion that the emission spectra have two components with different lifetimes which is evidenced by the time-resolved spectroscopies:[38,40] one from the vertical excited-state geometry, which possesses shorter excited-state lifetime, and the other from the relaxed excited-state geometry, which possesses much longer excited-state lifetime. Dual fluorescence resulting from these two conformations before and after the excited-state relaxation leads to the broad emission band, and both the two conformations have to be utilized to reproduce the observed broad feature.

In ref 24, the authors employed the time-dependent Hartree−Fock (TD-HF) method to describe the excited states and the redshift of the emission spectrum was only attributed to the change of the intermolecular relative orientation in the excited state. A much larger change on the intermolecular relative orientation was predicted in ref 24 than that in our work, which is reasonable since our model dimers are extracted from a rigidly linked structure. Our results demonstrate that the redshift of the

dx.doi.org/10.1021/jp107449v |J. Phys. Chem. B 2011, 115, 2699–2708

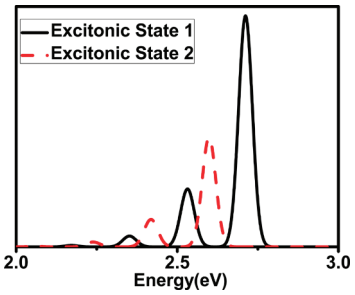

Figure 8. Calculated emission spectra of J-aggregated oligomers with two PBI units assuming that the excitonic state 1 or 2 is exclusively populated. The vertical axis is in arbitrary units.

emission spectrum is resulted from the contribution of CTEs and the change of intermolecular relative orientation as well. Because of the change of intermolecular relative orientation and intermolecular distance in the S_1 geometry, the mixing degree of FEs-CTEs increases, which is evidenced by the increased values of both t_e (t_h) and J. TD-HF approach usually overestimates the energies of intermolecular charge-transfer states which leads to CTEs decoupled with FEs. In our work, TD-LRC-DFT is used to calculate the excited states of the dimer. Both the energy-level order and the energy intervals of the excited states are correctly produced by this approach.[26,60] It is found that the energy of intermolecular CT excitation is close to that of intramolecular localized excitation, and thus the mixing of two-types of excitations can not be neglected. The increase of both t_e (t_h) and J gives rise to the low-energy emission. Therefore to produce the agreed experimentally measured emission spectra, one should consider the excited-state relaxation of dimer. Our conclusion that the emission bands come from two species before and after the relaxation is consistent with ref 24.

C. J-Aggregated Oligomers. The scan of the potential energy curves of the J-aggregated dimer along the torsional angle (shown in Figure 1) shows the ground-state and excited-state energy minima are near 89° and 90°, respectively. However, all these conformations have negative dipole−dipole coupling values, which can be easily seen from the head-to-tail configurations of the two transition dipoles of the monomers, and the general trends will not change here. So we take the geometry at 90° for the calculations below. The energy of intermolecular charge-transfer excitation produced from the CDFT approach[59] is 3.9140 eV at B3LYP/6-31G(d) level within Qchem[58] package, which is highly above the Frenkel exciton energy 2.7539 eV. Therefore the contribution of CTEs to low-lying excited states can be neglected in this case, and only FE model is enough to calculate the spectra. The calculated excitonic coupling value of J is −0.0595 eV.

As shown in the calculated absorption spectra of J-aggregated oligomers in Figure 7, the absorption spectra show a red-shift and the relative intensity of 0−0 peak increases with more aggregated units, which is consistent with the experiment.[39] The experimental absorption spectra of "a" series and "b" series both show the above trend; and the red-shift of the absorption spectra of "a" series is ∼0.049 eV for the dimer and ∼0.088 eV for the trimer, and the red-shift of the "b" series is ∼0.040 and ∼0.051 eV, while the corresponding values of the simulated absorption spectra are ∼0.043 and ∼0.063 eV, respectively.

The trends of the emission spectra with aggregation are the same as the absorption spectra: the 0−0 peak red-shifts and its relative intensity increases both at T = 0 and 300 K compared with the spectra of monomer. There are shoulder peaks near 2.60 and 2.41 eV in the emission spectra at 300 K, which can be ascribed to the emission from the second excitonic state. In order to explain this, we show the emission spectra of the J-aggregated dimer assuming the first or the second excitonic state is exclusively populated in Figure 8. As we can see, the shoulder peaks in the emission spectra of the dimer at 300 K just come from the emission of the second excitonic state, and this mechanism is just the same as shown before for rubrene multichromophores.[25]

V. CONCLUDING REMARKS

By combining TD-LRC-DFT and the mixed FE-CTE model, we calculate the vibronic spectra of both H- and J-aggregated PBI dyes. The following conclusions can be drawn from this work.

TD-LRC-DFT calculation has demonstrated that the low-lying excited states of H-aggregated PBI dyes possess both the nature of CTE and FE. The CT exciton has a significant contribution to the photophysical properties of the $\pi-\pi$ stacked PBI aggregates, which is evidenced by that PL channels involve self-trapped exciton states. Therefore, to correctly describe the electronic excitation and emission of $\pi-\pi$ stacked PBI dyes, one should go beyond the Frenkel exciton model.

By adopting the mixed FE-CTE model, we succeed in explaining the experimentally observed red-shift of the absorption spectra. The large Stokes shift of the emission spectra can be reproduced by our model, and it is induced by the asymmetric nature of the lowest excitonic state of the H-aggregated oligomers. And the experimentally observed broad emission bands come from two species with different geometrical conformations. This effect is identified with the experimentally observed different radiation lifetimes.

The calculations show that for J-aggregated PBI oligomers, the interactions of FEs induce the red-shift and the increase of the relative intensity of 0−0 peak of the absorption spectra with more aggregated units.

■ AUTHOR INFORMATION

Corresponding Author

*E-mail: liangwz@ustc.edu.cn.

Present Addresses

[§]Institute of Intelligent Machines, Chinese Academy of Sciences, Hefei 230031, China

■ ACKNOWLEDGMENT

Financial supports from National Science Foundation of China (Grant Nos. 20833003 and 21073168), the National Basic Research Program of China (Grant No. 2011CB808501) and Chinese Academy of Science are acknowledged.

■ REFERENCES

(1) McDermott, G.; Prince, S. M.; Freer, A. A.; Hawthornthwaite-Lawless, A. M.; Papiz, M. Z.; Cogdell, R. J.; Isaacs, N. W. *Nature* **1995**, *374*, 517.

(2) Koepke, J.; Hu, X.; Muenke, C.; Schulten, K.; Michel, H. *Structure* **1996**, *4*, 581.

(3) Cogdell, R. J.; Isaacs, N. W.; Freer, A. A.; Howard, T. D.; Gardiner, A. T.; Prince, S. M.; Papiz, M. Z. *FEBS Lett.* **2003**, *555*, 35.

(4) Herman, P.; Kleinekathofer, U.; Barvik, I.; Schreiber, M. *J. Lumin.* **2001**, *94*, 447.
(5) Dahlbom, M.; Pullerits, T.; Mukamel, S.; Sandstrom, V. *J. Phys. Chem. B* **2001**, *105*, 5515.
(6) Zhao, Y.; Ng, M. F.; Chen, G. H. *Phys. Rev. E* **2004**, *69*, 032902.
(7) Lewis, F. D.; Kalgutkar, R. S.; Wu, Y.; Liu, X.; Liu, J.; Hayes, R. T.; Miller, S. E.; Wasielewski, M. R. *J. Am. Chem. Soc.* **2000**, *122*, 12346.
(8) Lewis, F. D.; Liu, J.; Weigel, W.; Rettig, W.; Kurnikov, I. V.; Beratan, D. N. *Proc. Natl. Acad. Sci. U.S.A.* **2002**, *99*, 12536.
(9) Lewis, F. D.; Wu, T.; Zhang, Y.; Letsinger, R. L.; Greenfield, S. R.; Wasielewski, M. R. *Science* **1997**, *277*, 673.
(10) Hu, L. H.; Zhao, Y.; Wang, F.; Chen, G. H.; Ma, C. S.; Kwork, W. M.; Phillips, D. L. *J. Phys. Chem. B* **2007**, *111*, 11812.
(11) Herbst, W.; Hunger, K. *Industrial Organic Pigments: Production, Properties, Applications*, 2nd ed.; Wiley-VCH: Weinheim, Germany, 1997.
(12) Würthner, F. *Chem. Commun.* **2004**, 1564, and references therein.
(13) Gautier, N.; Dumur, F.; Lloveras, V.; Gancedo, J. V.; Veciana, J.; Rovira, C.; Hudhomme, P. *Angew. Chem., Int. Ed.* **2003**, *42*, 2765.
(14) Cukier, R. I.; Nocera, D. G. *Annu. Rev. Phys. Chem.* **1998**, *49*, 337.
(15) Schlicke, B.; Belser, P.; Cola, L. D.; Sabbioni, E.; Balzani, V. *J. Am. Chem. Soc.* **1999**, *121*, 4207.
(16) D'Aléo, A.; Welter, S.; Cecchetto, E.; Cola, L. D. *Pure Appl. Chem.* **2005**, *77*, 1035.
(17) Curutchet, C.; Mennucci, B. *J. Am. Chem. Soc.* **2005**, *127*, 16733.
(18) Cornil, J.; Beljonne, D.; Calbert, J.-P.; Brȩdas, J.-L. *AdV. Mater.* **2001**, *13*, 1053.
(19) Spano, F. C. *Annu. ReV. Phys. Chem.* **2006**, *57*, 217.
(20) Renger, T.; Voigt, J.; May, V.; Kühn, O. *J. Phys. Chem.* **1996**, *100*, 15654.
(21) Seibt, J.; Dehm, V.; Würthner, F.; Engel, V. *J. Chem. Phys.* **2007**, *126*, 164308.
(22) Seibt, J.; Engel, V. *Chem. Phys.* **2008**, *347*, 120.
(23) Seibt, J.; Marquetand, P.; Engel, V.; Chen, Z.; Dehm, V.; Würthner, F. *Chem. Phys.* **2006**, *328*, 354.
(24) Fink, R. F.; Seibt, J.; Engel, V.; Renz, M.; Kaupp, M.; Lochbrunner, S.; Zhao, H.-M.; Pfister, J.; Würthner, F.; Engels, B. *J. Am. Chem. Soc.* **2008**, *130*, 12858.
(25) Gao, F.; Liang, W. Z.; Zhao, Y. *J. Phys. Chem. A* **2009**, *113*, 12847.
(26) Pan, F.; Gao, F.; Liang, W. Z.; Zhao, Y. *J. Phys. Chem. B* **2009**, *113*, 14581.
(27) Chen, Z.; Stepanenko, V.; Dehm, V.; Prins, P.; Siebbeles, L. D. A.; Seibt, J.; Marquetand, P.; Engel, V.; Würthner, F. *Chem.—Eur. J.* **2007**, *13*, 436.
(28) Li, A. D. Q.; Wang, W.; Wang, L. Q. *Chem.—Eur. J.* **2003**, *9*, 4594.
(29) Wang, W.; Li, L. S.; Helms, G.; Zhou, H. H.; Li, A. D. Q. *J. Am. Chem. Soc.* **2003**, *125*, 1120.
(30) Han, J. J.; Shaller, A. D.; Wang, W.; Li, A. D. Q. *J. Am. Chem. Soc.* **2008**, *130*, 6974.
(31) Clark, A. E.; Qin, C.; Li, A. D. Q. *J. Am. Chem. Soc.* **2007**, *129*, 7586.
(32) Scholz, R.; Kobitski, A. Y.; Kampen, T. U.; Schreiber, M.; Zahn, D. R. T. *Phys. Rev. B* **2000**, *61*, 13659.
(33) Forrest, S. R. *Chem. Rev.* **1997**, *97*, 1793.
(34) Scholz, R.; Kobitski, A. Y.; Zahn, D. R. T.; Schreiber, M. *Phys. Rev. B* **2005**, *72*, 245208.
(35) Hoffmann, M.; Soos, Z. G. *Phys. Rev. B* **2002**, *66*, 024305.
(36) Mazur, G.; Petelenz, P.; Slawik, M. *J. Chem. Phys.* **2003**, *118*, 1423.
(37) Tsiper, E. V.; Soos, Z. G. *Phys. Rev. B* **2001**, *64*, 195124.
(38) Giaimo, J. M.; Lockard, J. V.; Sinks, L. E.; Scott, A. M.; Wilson, T. M.; Wasielewski, M. R. *J. Phys. Chem. A* **2008**, *112*, 2322.
(39) Wilson, T. M.; Tauber, M. J.; Wasielewski, M. R. *J. Am. Chem. Soc.* **2009**, *131*, 8952.
(40) Veldman, D.; Chopin, S. M. A.; Meskers, S. C. J.; Groeneveld, M. M.; Williams, R. M.; Janssen, R. A. J. *J. Phys. Chem. A* **2008**, *112*, 5846.
(41) Ahrens, M. J.; Sinks, L. E.; Rybtchinski, B.; Liu, W. H.; Jones, B. A.; Giaimo, J. M.; Gusev, A. V.; Goshe, A. J.; Tiede, D. M.; Wasielewski, M. R. *J. Am. Chem. Soc.* **2004**, *126*, 8284.
(42) Yagai, S.; Seki, T.; Karatsu, T.; Kitamura, A.; Würthner, F. *Angew. Chem., Int. Ed.* **2008**, *47*, 3367.
(43) Hoffmann, M.; Schmidt, K.; Fritz, T.; Hasche, T.; Agranovich, V. M.; Leo, K. *Chem. Phys.* **2000**, *258*, 73.
(44) McWeeny, R. *Methods of Molecular Quantum Mechanics*, 2nd ed.; Academic Press: London, 1992.
(45) Hsu, C.-P.; Fleming, G. R.; Head-Gordon, M.; Head-Gordon, T. *J. Chem. Phys.* **2001**, *114*, 3065.
(46) Scholes, G. D. *Annu. Rev. Phys. Chem.* **2003**, *54*, 57.
(47) Scholes, G. D.; Harcourt, R. D.; Ghiggino, K. P. *J. Chem. Phys.* **1995**, *102*, 9574.
(48) Thompson, A. L.; Gaab, K. M.; Xu, J.; Bardeen, C. J.; Martinez, T. J. *J. Phys. Chem. A* **2004**, *108*, 671.
(49) Merrifield, R. E. *J. Chem. Phys.* **1961**, *31*, 1835.
(50) Lalov, I. J.; Warns, C.; Reineker, P. *New J. Phys.* **2008**, *10*, 085006.
(51) Senthilkumar, K.; Grozema, F. C.; Guerra, C. F.; Bichelhaupt, F. M.; Lewis, F. D.; Berlin, Y. A.; Ratner, M. A.; Siebbeles, L. D. *J. Am. Chem. Soc.* **2005**, *127*, 14894.
(52) Valeev, E. F.; Coropceanu, V.; da Silva Filho, D. A.; Salman, S.; Brédas, J. L. *J. Am. Chem. Soc.* **2006**, *128*, 9882.
(53) Li, H.; Bredas, J. L.; Lennartz, C. *J. Chem. Phys.* **2007**, *126*, 164704.
(54) Ahlrichs, R.; Bär, M.; Baron, H.-P.; Bauernschmitt, R.; Böcker, S.; Deglmann, P.; Ehrig, M.; Eichkorn, K.; Elliott, S.; Furche, F.; Haase, F.; Häser, M.; Horn, H.; Hättig, C.; Huber, C.; Huniar, U.; Kattannek, M.; Andreas Köhn, A.; Kölmel, C.; Kollwitz, M.; May, K.; Ochsenfeld, C.; Ohm, H.; Patzelt, H.; Rubner, O.; Schafer, S.; Schneider, U.; Sierka, M.; Treutler, O.; Unterreiner, B.; von Arnim, M.; Weigend, F.; Weis, P.; Weiss, H. *TURBOMOLE*; Quantum Chemistry Group, Universität Karlsruhe, 2003; Ver5.6.
(55) Zhao, Y.; Liang, W. Z.; Nakamura, H. *J. Phys. Chem. A* **2006**, *110*, 8204.
(56) (a) Chai, J.-D.; Head-Gordon, M. *J. Chem. Phys.* **2008**, *128*, 084106. (b) Chai, J.-D.; Head-Gordon, M. *Chem. Phys. Lett.* **2008**, *467*, 176.
(57) Frisch, M. J.; Trucks, G. W.; Schlegel, H. B.; Scuseria, G. E.; Robb, M. A.; Cheeseman, J. R.; Montgomery Jr, J. A.; Vreven, T.; Kudin, K. N.; Burant, J. C.; Millam, J. M.; Iyengar, S. S.; Tomasi, J.; Barone, V.; Mennucci, B.; Cossi, M.; Scalmani, G.; Rega, N.; Petersson, G. A.; Nakatsuji, H.; Hada, M.; Ehara, M.; Toyota, K.; Fukuda, R.; Hasegawa, J.; Ishida, M.; Nakajima, T.; Honda, Y.; Kitao, O.; Nakai, H.; Klene, M.; Li, X.; Knox, J. E.; Hratchian, H. P.; Cross, J. B.; Bakken, V.; Adamo, C.; Jaramillo, J.; Gomperts, R.; Stratmann, R. E.; Yazyev, O.; Austin, A. J.; Cammi, R.; Pomelli, C.; Ochterski, J. W.; Ayala, P. Y.; Morokuma, K.; Voth, G. A.; Salvador, P.; Dannenberg, J. J.; Zakrzewski, V. G.; Dapprich, S.; Daniels, A. D.; Strain, M. C.; Farkas, O.; Malick, D. K.; Rabuck, A. D.; Raghavachari, K.; Foresman, J. B.; Ortiz, J. V.; Cui, Q.; Baboul, A. G.; Clifford, S.; Cioslowski, J.; Stefanov, B. B.; Liu, G.; Liashenko, A.; Piskorz, P.; Komaromi, I.; Martin, R. L.; Fox, D. J.; Keith, T.; Al-Laham, M. A.; Peng, C. Y.; Nanayakkara, A.; Challacombe, M.; Gill, P. M. W.; Johnson, B.; Chen, W.; Wong, M. W.; Gonzalez, C.; Pople, J. A. Gaussian 03; Gaussian: Pittsburgh, PA, 2003.
(58) Shao, Y.; Molnar, L. F.; Jung, Y.; Kussmann, J.; Ochsenfeld, C.; Brown, S. T.; Gilbert, A. T. B.; Slipchenko, L. V.; Levchenko, S. V.; ONeill, D. P.; DiStasio, R. A.; Lochan, R. C.; Wang, T.; Beran, G. J. O.; Besley, N. A.; Herbert, J. M.; Lin, C. Y.; Van Voorhis, T.; Chien, S. H.; Sodt, A.; Steele, R. P.; Rassolov, V. A.; Maslen, P. E.; Korambath, P. P.; Adamson, R. D.; Austin, B.; Baker, J.; Byrd, E. F. C.; Dachsel, H.; Doerksen, R. J.; Dreuw, A.; Dunietz, B. D.; Dutoi, A. D.; Furlani, T. R.; Gwaltney, S. R.; Heyden, A.; Hirata, S.; Hsu, C. P.; Kedziora, G.; Khalliulin, R. Z.; Klunzinger, P.; Lee, A. M.; Lee, M. S.; Liang, W.; Lotan, I.; Nair, N.; Peters, B.; Proynov, E. I.; Pieniazek, P. A.; Rhee, Y. M.;

Ritchie, J.; Rosta, E.; Sherrill, C. D.; Simmonett, A. C.; Subotnik, J. E.; Woodcock, H. L.; Zhang, W.; Bell, A. T.; Chakraborty, A. K.; Chipman, D. M.; Keil, F. J.; Warshel, A.; Hehre, W. J.; Schaefer, H. F.; Kong, J.; Krylov, A. I.; Gill, P. M. W.; Head-Gordon, M. *Phys. Chem. Chem. Phys.* **2006**, *8*, 3172.

(59) Wu, Q.; Van Voorhis, T. *J. Chem. Phys.* **2006**, *125*, 164105.

(60) Song, J.; Gao, F.; Shi, B.; Liang, W. Z. *Phys. Chem. Chem. Phys.* **2010**, *12*, 13070.